

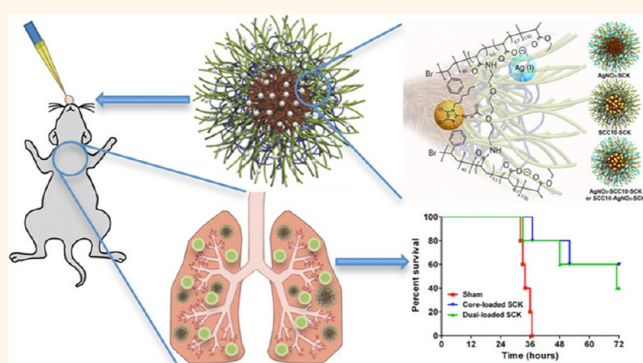
Synthesis, Characterization, and *In Vivo* Efficacy of Shell Cross-Linked Nanoparticle Formulations Carrying Silver Antimicrobials as Aerosolized Therapeutics

Parth N. Shah,^{†,#} Lily Yun Lin,^{‡,#,¶} Justin A. Smolen,[†] Jasur A. Tagaev,[†] Sean P. Gunsten,[§] Daniel S. Han,[†] Gyu Seong Heo,[‡] Yali Li,[△] Fuwu Zhang,[‡] Shiyi Zhang,[‡] Brian D. Wright,^{||} Matthew J. Panzner,^{||} Wiley J. Youngs,^{||} Steven L. Brody,[§] Karen L. Wooley,^{‡,*} and Carolyn L. Cannon^{†,*}

[†]Department of Pediatrics, Division of Pulmonary and Vascular Biology, University of Texas Southwestern Medical Center, Dallas, Texas 75390, United States,

[‡]Departments of Chemistry and Chemical Engineering, Texas A&M University, P.O. Box 30012, College Station, Texas 77842, United States, [§]Department of Internal Medicine, Division of Pulmonary and Critical Care Medicine, Washington University School of Medicine, St. Louis, Missouri 63110, United States, ^{||}Department of Pediatrics, Division of Allergy, Immunology, and Pulmonary Medicine, Washington University School of Medicine, St. Louis, Missouri 63110, United States, and [△]Center for Silver Therapeutics Research, Department of Chemistry, The University of Akron, Akron, Ohio 44325-3601, United States. [#]These authors contributed equally to this work. ^{*}Present address: Laboratory for Biomaterials and Drug Delivery, Department of Anesthesiology, Division of Critical Care Medicine, Children's Hospital Boston, Harvard Medical School, 300 Longwood Avenue, Boston, MA 02115. [¶]Present address: Waters Corporation, 34 Maple Street, Milford, MA 01757-3696.

ABSTRACT The use of nebulizable, nanoparticle-based antimicrobial delivery systems can improve efficacy and reduce toxicity for treatment of multi-drug-resistant bacteria in the chronically infected lungs of cystic fibrosis patients. Nanoparticle vehicles are particularly useful for applying broad-spectrum silver-based antimicrobials, for instance, to improve the residence time of small-molecule silver carbene complexes (SCCs) within the lung. Therefore, we have synthesized multifunctional, shell cross-linked knedel-like polymeric nanoparticles (SCK NPs) and capitalized on the ability to independently load the shell and core with silver-based antimicrobial agents. We formulated three silver-loaded variants of SCK NPs: shell-loaded with silver cations, core-loaded with SCC10, and combined loading of shell silver cations and core SCC10. All three formulations provided a sustained delivery of silver over the course of at least 2–4 days. The two SCK NP formulations with SCC10 loaded in the core each exhibited excellent antimicrobial activity and efficacy *in vivo* in a mouse model of *Pseudomonas aeruginosa* pneumonia. SCK NPs with shell silver cation-load only, while efficacious *in vitro*, failed to demonstrate efficacy *in vivo*. However, a single dose of core SCC10-loaded SCK NPs (0.74 ± 0.16 mg Ag) provided a 28% survival advantage over sham treatment, and administration of two doses (0.88 mg Ag) improved survival to 60%. In contrast, a total of 14.5 mg of Ag⁺ delivered over 5 doses at 12 h intervals was necessary to achieve a 60% survival advantage with a free-drug (SCC1) formulation. Thus, SCK NPs show promise for clinical impact by greatly reducing antimicrobial dosage and dosing frequency, which could minimize toxicity and improve patient adherence.



KEYWORDS: shell cross-linked knedel-like polymeric nanoparticles · silver carbene complexes · cystic fibrosis · nebulizable nanoparticles · multi-drug-resistant bacteria · *Pseudomonas aeruginosa* pneumonia

Cystic fibrosis (CF) results from mutation of the cystic fibrosis transmembrane conductance regulator (CFTR) gene,¹ affects about 70 000 humans worldwide,¹ and is the most common life-shortening genetic disease among Caucasians.² This disease affects multiple organs including the lungs and upper respiratory tract, the gastrointestinal tract, pancreas, liver, sweat

glands, and genitourinary tract. A major feature of the CF disease of the airway is disruption of the normal airway fluid and mucus secretion.¹ Consequently, pathogenic bacteria can easily colonize and persist in the airway and form biofilms. A variety of opportunistic pathogens, including *Pseudomonas aeruginosa*, *Staphylococcus aureus*, and *Burkholderia cepacia* complex (Bcc),

* Address correspondence to wooley@chem.tamu.edu, carolyn.cannon@utsouthwestern.edu.

Received for review January 21, 2013 and accepted May 29, 2013.

Published online May 29, 2013
10.1021/nn400322f

© 2013 American Chemical Society

cause chronic pulmonary infections and subsequently result in intense persistent inflammation, which is a major cause of the morbidity and mortality in these patients.¹ Furthermore, the ability of these organisms to form biofilms renders them resistant to eradication, even with aggressive therapy comprising frequent high-dose administration of intravenous antibiotics, such as aminoglycosides and β -lactams. In the case of *P. aeruginosa*, phenotypic variants with an enhanced capacity for biofilm formation are also highly antibiotic-resistant compared with the parent strains.^{3,4} Similarly, the proportion of CF patients colonized with methicillin-resistant *Staphylococcus aureus* (MRSA) continues to escalate.^{5,6} Colonization with Bcc poses a life-threatening problem, as they are inherently antibiotic resistant.⁷ Furthermore, the frequent administration of intravenous high-dose antibiotics used as the current mainstay of therapy can potentially result in severe side effects.⁸ Therefore, to combat the problems associated with toxicity and antimicrobial resistance, there is a great need for finding new modalities of treatment.⁹

Silver, an agent with a historical significance for use in controlling infections, has been demonstrated to be highly biocidal against bacteria, including *Pseudomonas aeruginosa*, *Staphylococcus aureus*, and *Escherichia coli*, as well as fungal pathogens.¹⁰ Presently, silver compounds are used as antimicrobial agents for the treatment of wounds and burns,^{11,12} as coatings for catheters and endotracheal tubes, and as disinfectants.^{13,14} In addition to its broad-spectrum antimicrobial activity, the relatively few reported accounts of silver resistance, despite its widespread and continuous use,^{15–19} and the low toxicity of Ag^+ to human tissues^{11,15,18} make silver-based antimicrobials very attractive. Hence, there has been a recent resurgence in the development of silver-based systems for antimicrobial applications. For instance, Sen and co-workers²⁰ have formulated poly(4-vinyl-N-hexylpyridinium bromide) cationic polymer/silver bromide nanoparticle composites, whereas hybrids of silver nanoparticles and amphiphilic hyperbranched macromolecules composed of polyethyleneimine have been developed by Tiller, Mecking, and co-workers.²¹ Recently, Mahmoudi and Serpooshan have devised a novel system comprising ultrathin silver ring-coated superparamagnetic iron oxide nanoparticles (SPIONs) with ligand gaps that demonstrate excellent antimicrobial activity against *Staphylococcus aureus* and *Staphylococcus epidermidis* biofilms while maintaining compatibility with human cells, thus alleviating the toxicity-related problems associated with silver nanoparticles.²²

Members of our research group have synthesized and characterized a series of N-heterocyclic silver carbene complexes (SCCs)^{23–28} and demonstrated their activity against a wide variety of Gram-positive and Gram-negative pathogens, including antibiotic-resistant *P. aeruginosa*, methicillin-resistant *Staphylococcus aureus*,

and *Burkholderia* species isolated from the lungs of CF patients, as well as weaponizable BSL3 bacteria.^{23–28} The SCCs are easily nebulized or aerosolized, providing a means for direct administration to the lung *via* inhalation—an efficacious method for localized delivery to the site of infection.^{29,30} Nebulization allows for the achievement of therapeutic outcomes with higher local drug concentration due to high doses delivered to the lung, a proportionally lower systemic drug concentration, and therefore decreased systemic toxicity.^{31,32} However, the small size of SCCs and their quick diffusion across lung epithelium results in rapid clearance from the lungs following administration.^{29,30} Instead of relying on patient adherence for several repeated inhaled dosages to maintain effective therapeutic concentrations within the lung, a strategy that may pose problems, we have sought to investigate the use of inhaled nanoparticles loaded with SCCs.

Cannon and Youngs *et al.* have reported the sustained release of SCC10 from L-tyrosine polyphosphate (LTP) nanoparticles and demonstrated their antimicrobial efficacy both *in vitro* and *in vivo*.³¹ To improve upon the capabilities of the LTP nanoparticles, we have developed multifunctional, shell cross-linked knedel-like polymeric nanoparticles (SCK NPs) that are optimized for encapsulation and delivery of silver cations and/or SCCs.³³ The SCK NPs are composed of an amphiphilic diblock copolymer, poly(acrylic acid)-*b*-polystyrene (PAA-*b*-PS), which allows for the encapsulation of hydrophobic silver carbene complexes within the hydrophobic polystyrene core of the nanoparticles and the complexation of silver cation to the hydrophilic poly(acrylic acid) presented on the shell of the nanoparticles (Figure 1). Furthermore, compared with the LTP nanoparticles,³¹ the SCK NPs are of significantly lower particle size and provide functionalities at the nanoparticle surface for the attachment of targeting moieties. Previous *in vitro* studies of the silver-loaded SCK NPs have demonstrated excellent antibacterial activity.³⁴ Prior to *in vivo* efficacy studies, we first have confirmed that SCK NPs do not elicit an inflammatory response in the lungs of mice following intratracheal instillation. Subsequently, we have demonstrated the therapeutic efficacy of nebulized silver-loaded SCKs in a mouse model of *P. aeruginosa* pneumonia. Finally, in the same *in vivo* model of *P. aeruginosa* pneumonia, we have compared the efficacy of core-loaded SCK NPs to that of the shell-loaded and dual-loaded SCK NPs and have observed an apparent superiority of the core-loaded SCK NP formulation.

RESULTS AND DISCUSSION

The dimensions of all silver-loaded SCK NPs were characterized by transmission electron microscopy (TEM) and dynamic light scattering (DLS). As a comparison, empty SCK NPs without silver were also characterized.

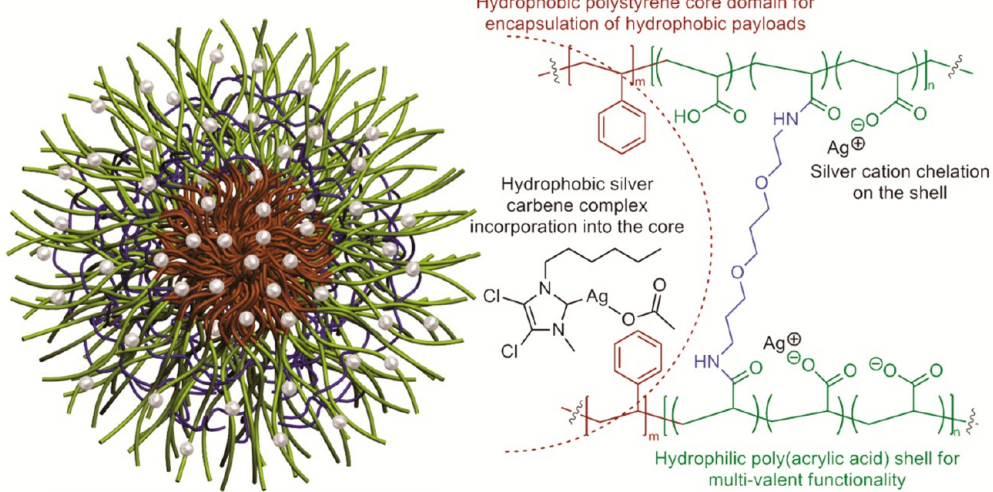


Figure 1. Schematic (left) and chemical representation (right) of a shell cross-linked nanoparticle (SCK NP, cross-linkers are represented as blue rod) assembled from poly(acrylic acid)_n-*b*-polystyrene_m (diblock copolymer represented by green (PAA) and brown (PS) rod) loaded with silver carbene complexes in the core and silver cation in the shell (represented by silver balls), where $n = 120$ and $m = 40$.

The well-defined circularly shaped images observed by TEM suggested that the empty SCK NPs were spherical, with a narrow size distribution of 14 ± 3 nm (Figure 2, Table 1). Silver-loaded SCK NPs were also spherical with comparable sizes and size distributions, indicating that the silver incorporation did not affect the size or the shape of the SCK NPs. Their number-average hydrodynamic diameters, characterized by DLS, were also similar across loading methods, ~ 24 – 30 nm, with narrow number-average size distributions of ~ 6 – 8 nm (Figure 3, Table 1).

To better understand where the silver species reside, we performed both dark- and bright-field scanning transmission electron microscopy (STEM) on unstained AgNO_3 -SCK and SCC10-SCK and observed the contrast enhancement due to the presence of silver. The dark-field STEM image of AgNO_3 -SCK (Figure 4A) showed that the shell of the nanoparticle was more illuminated compared with the core of the nanoparticle, due to the silver cations in the shell. This observation strongly supported our hypothesis that the silver cations from the AgNO_3 is more likely to complex with the acrylic acid residues throughout the shells of the nanoparticles. In the case of SCC10-SCK, the SCC10 is hydrophobic and more likely to be localized in the core of the nanoparticles. Indeed, the cores of the nanoparticles were preferentially illuminated as demonstrated by STEM images (Figure 4B). The bright-field STEM images also showed the incorporation of the silver species into the nanoparticles (Figure 4C,D).

SCK Induces No Acute Inflammatory Response in the Lung Following Intratracheal Delivery. Before investigating the efficacy of the silver-loaded SCK NPs in an infection model, we sought to determine whether or not the empty SCKs elicited an inflammatory response, which would indicate undesirable toxicity. Thus, SCK NPs in

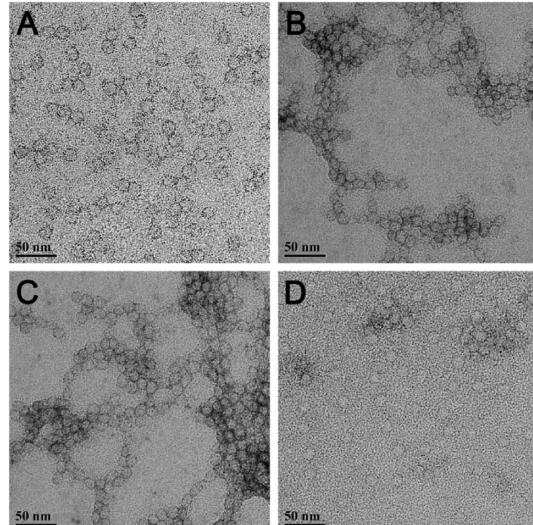


Figure 2. TEM images (drop deposited on carbon-coated copper grids and stained negatively with 1% aqueous uranyl acetate) of (A) empty SCK NPs, (B) AgNO_3 -SCK, (C) AgCOOCH_3 -SCK, and (D) SCC10-SCK.

phosphate buffered saline (PBS) were administered to mice intratracheally, and the inflammatory response was analyzed 24 h later by quantifying inflammatory cells recovered in bronchoalveolar lavage (BAL) fluid. The total number of cells recovered from BAL was not significantly different ($p = 0.354$) than that of mice receiving PBS alone. Further, evaluation of BAL cell types collected from SCK-treated animals resulted in no significant difference in total numbers of macrophages ($p = 0.391$), lymphocytes ($p = 0.772$), or neutrophils ($p = 0.126$) as compared to mice treated with only PBS (Figure 5).

In Vivo Evaluation of the Antimicrobial Efficacy of SCK NPs. Once the SCK NPs demonstrated a lack of inflammatory response (response comparable to PBS) upon acute

TABLE 1. Summary of Characterization Data for Empty and Silver-Loaded SCK NPs Measured by TEM and DLS

| | diameter by TEM (nm) | D_h (intensity) (nm) | D_h (volume) (nm) | D_h (number) (nm) | DLS PDI |
|---------------------------|----------------------|------------------------|---------------------|---------------------|---------|
| empty SCK | 14 \pm 3 | 180 \pm 110 | 50 \pm 30 | 30 \pm 8 | 0.302 |
| AgNO ₃ -SCK | 14 \pm 2 | 140 \pm 90 | 35 \pm 20 | 24 \pm 6 | 0.279 |
| AgCOOCH ₃ -SCK | 13 \pm 3 | 150 \pm 120 | 40 \pm 20 | 25 \pm 7 | 0.289 |
| SCC10-SCK | 15 \pm 4 | 150 \pm 120 | 40 \pm 25 | 28 \pm 8 | 0.290 |

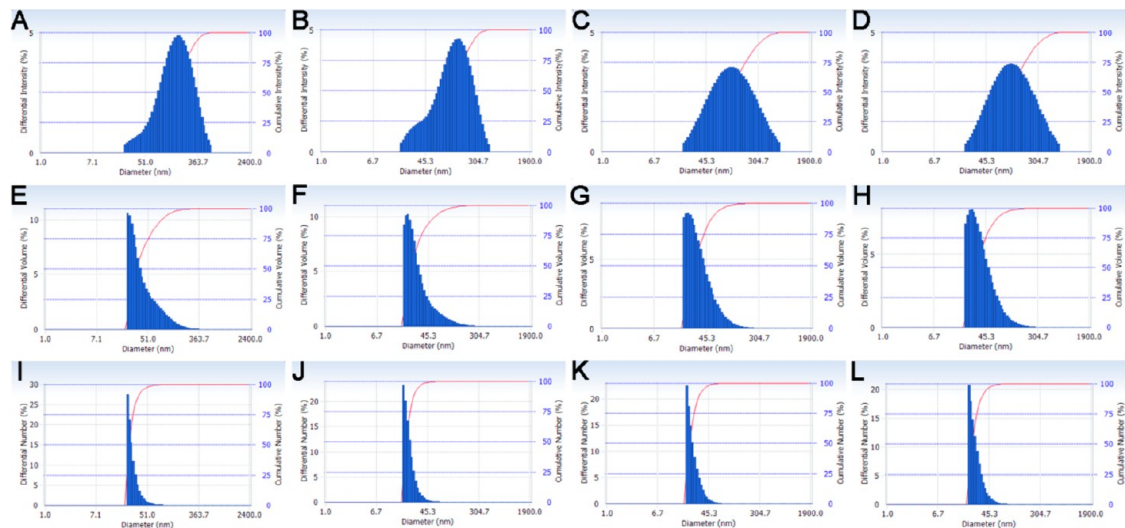


Figure 3. Dynamic light scattering histograms (determinations were average values from 10 measurements, with the standard deviations being calculated as the breadth of the distributions). Top row: intensity average of (A) empty SCK, (B) AgNO₃-SCK, (C) AgCOOCH₃-SCK, and (D) SCC10-SCK. Middle row: volume average of (E) empty SCK, (F) AgNO₃-SCK, (G) AgCOOCH₃-SCK, and (H) SCC10-SCK. Bottom row: number-average of (I) empty SCK, (J) AgNO₃-SCK, (K) AgCOOCH₃-SCK, and (L) SCC10-SCK.

intratracheal delivery in mice, we began an initial evaluation of the *in vivo* antimicrobial effects of the SCKs. Survival studies were conducted to compare the efficacy of the shell-loaded SCK NPs to the core-loaded SCK NPs using a *P. aeruginosa* murine infection model. In addition to survival, weight loss and clinical scores were used as other markers of efficacy. The animals were delivered a single dose of nebulized treatment in a nose-only fashion 1 h post-inoculation. The corresponding total dose of silver ions delivered for the core-loaded SCK NPs (SCC10-SCK) and the shell-loaded SCK NPs (AgNO₃-SCK/AgCOOCH₃-SCK) was 0.74 \pm 0.16 and 1.22 \pm 0.33 mg of Ag⁺, respectively. All animals lost weight following *P. aeruginosa* infection; however, by 48 h, the animals treated with core-loaded SCK NPs that had survived had started to regain weight. The manifestation and progression of infection was also evident from the clinical scores of the animals. The mean clinical score for sham-treated animals was the highest at any given time point, followed by the mean score for shell-loaded SCK-NP-treated animals, whereas core-loaded SCK-NP-treated animals exhibited the lowest score ($p = 0.067$ compared with shell-loaded SCK NPs, $p = 0.014$ compared with sham). Although there was no statistical difference between the clinical scores of animals treated with various silver-containing SCK NP

formulations at 24 h, the scores of all animals, except those treated with core-loaded SCK NPs, progressively worsened with time. Consequently, 100% lethality was observed in both sham-treated and shell-loaded SCK-NP-treated animals by approximately 48 h post-inoculation. However, treatment with core-loaded SCK NPs resulted in a 28% survival advantage ($p = 0.0582, 0.14$). These results demonstrate a distinct trend indicating the superiority of core-loaded SCK NPs for the treatment of *P. aeruginosa* associated pneumonia (Figure 6). Furthermore, a contingency analysis of the data corroborated these findings and demonstrated a statistically significant survival advantage conferred by the treatment of core-loaded SCK NPs compared with shell-loaded SCK NPs (Figure 7, $p = 0.037$). These results are surprising because the measured dosage of Ag⁺ ions delivered with the shell-loaded SCK NPs was approximately 2-fold higher than the Ag⁺ dose delivered by core-loaded SCK NPs.

Subsequent studies were performed to compare the *in vivo* efficacy of core-loaded SCK NPs (SCC10-SCK) to the dual-loaded SCK NPs³⁴ (SCC10-AgNO₃-SCK with silver loading in the core and the shell). Two doses of aerosolized core-loaded SCK NPs and dual-loaded SCK NPs were delivered 24 h apart in a nose-only manner to *P. aeruginosa*-infected mice in a multi-dosing chamber

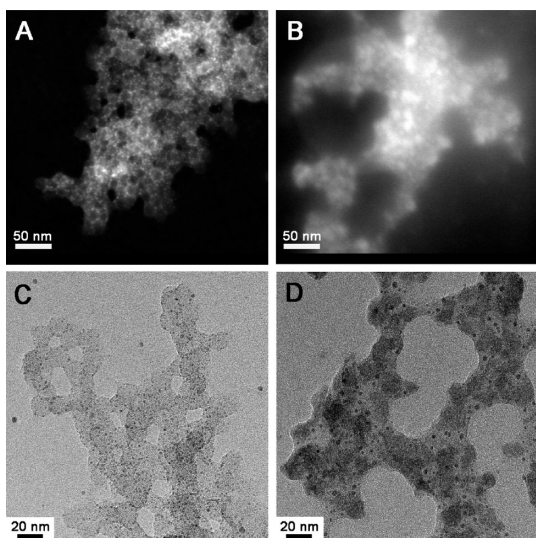


Figure 4. STEM dark-field images (drop deposited on carbon-coated copper grids with no stain) of (A) AgNO_3 -SCK and (B) SCC10-SCK. STEM bright-field images (drop deposited on carbon-coated copper grids with no stain) of (C) AgNO_3 -SCK and (D) SCC10-SCK.

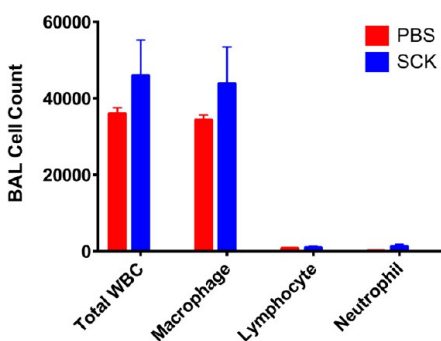


Figure 5. Effect of intratracheal instillation of PBS or SCK NPs in PBS on inflammatory cell differentials in bronchoalveolar lavage (BAL) fluid in mice. Cytospin preparations of cell pellets prepared from BAL fluid and light microscopy analysis were used to determine cell differentials, which demonstrates no significant differences between total inflammatory cell counts or individual cell types recovered from mice treated with PBS or SCK NPs in PBS.

(Figure 8). The corresponding total dose per treatment of silver for the core-loaded SCK NPs and dual-loaded SCK NPs was 0.44 and 0.71 mg of Ag, respectively. LD_{100} was achieved in mice that were provided sham treatment, with 100% lethality occurring by approximately 36 h post-inoculation. Treatment with core-loaded SCK NPs resulted in a 60% survival advantage ($p = 0.002$), whereas treatment with dual-loaded SCK NPs resulted in a 40% survival advantage, compared with sham-treated animals ($p = 0.021$). Unexpectedly, considerably lower silver loading within the core-loaded SCK NPs ($\sim 1/2$ of the dual-loaded SCK NPs) did not result in a lower survival advantage compared with dual-loaded SCK NP formulation, which demonstrated a 20% lower yet nonsignificantly different survival advantage ($p = 0.57$).

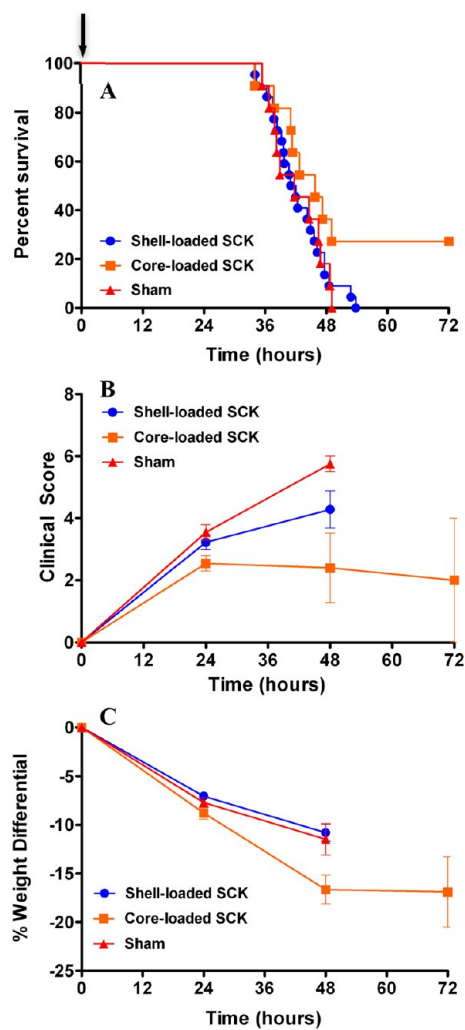


Figure 6. Effect of nebulized SCK NPs on survival, weight loss, and clinical scores in a mouse model of *P. aeruginosa* infection. Mice were infected intranasally with 1.2×10^6 CFU per mouse of a clinical mucoid strain of *P. aeruginosa* (PA M57-15) and subsequently received a single-dose treatment with shell-loaded SCK NPs, core-loaded SCK NPs, or phosphate buffer vehicle 1 h after infection (as indicated by an arrow in panel A). (A) Kaplan-Meier survival curves. The survival of mice treated with core-loaded SCK NPs was greater than that of those treated with shell-loaded SCK NPs and phosphate buffer vehicle. (B) Clinical score. The mice treated with core-loaded SCK NPs exhibited better scores compared with animals treated with shell-loaded SCK NPs and phosphate buffer vehicle. (C) Weight loss. Mice treated with core-loaded SCK NPs lost slightly more weight than animals treated with shell-loaded SCKs and phosphate buffer vehicle at 48 h.

These results illustrate that the core-loaded SCK NP and dual-loaded SCK NP formulations are effective against CF-relevant bacteria *P. aeruginosa* and can be used to reduce the likelihood of death in a *P. aeruginosa* pneumonia model. A 28% survival advantage was observed upon treatment with core-loaded SCK NPs over any other treatment in the case of a murine infection model experiment comparing the efficacy of the core-loaded NPs (SCC10-SCK) to the shell-loaded NPs (AgNO_3 -SCK and AgCOOCH_3 -SCK). A comparison

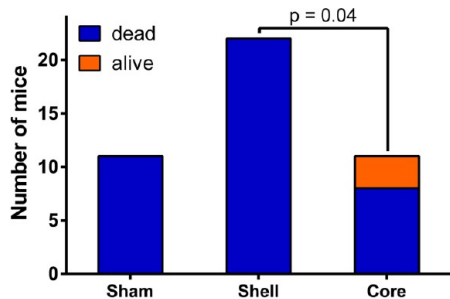


Figure 7. Contingency analysis of survival data using Fisher's exact test demonstrating the superiority of core-loaded SCK NPs compared with shell-loaded SCK NPs for treating *P. aeruginosa*-associated pneumonia.

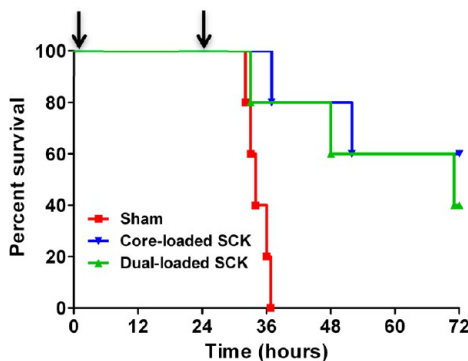


Figure 8. Kaplan-Meier survival curves demonstrating the superiority of core-loaded SCK NPs compared with dual-loaded SCK NPs and sham treatment in a mouse model of *P. aeruginosa* infection. Mice were infected intranasally with 1.3×10^6 CFU per mouse of a clinical mucoid strain of *P. aeruginosa* (PA M57-15) and subsequently received two treatments with core-loaded SCK NPs, dual-loaded SCK NPs, or phosphate buffer vehicle 1 and 25 h after infection (as indicated by arrows). The survival of mice treated with core-loaded SCK NPs was greater than that of those treated with dual-loaded SCK NPs or phosphate buffer vehicle.

of the release characteristics of silver from the nanoparticle formulations indicates that the core-loaded SCK NPs and the shell-loaded SCK NPs each provide a similar, relatively slow, and sustained release of silver.³⁴ For each formulation, approximately 50% of the silver is released over the first 24 h and a cumulative release of 80% of the encapsulated silver occurs by the second day. While the release rate of a drug from NPs is important in achieving therapeutic effect in most instances, a lack of significant difference in the release rate of silver from different SCK NP formulations suggests that the release rate is not a limiting parameter in this instance. Therefore, the superior therapeutic efficacy associated with the core-loaded SCK NPs, despite their lower Ag⁺ loading, may be attributed to the stability of the silver carbene complex or other factors, as yet unknown.

The shell-loaded AgNO₃-SCK and AgCOOCH₃-SCK NPs are expected to release silver as the incorporated salt or the silver cation, and in addition, Ag⁰ has been observed to accumulate near the shell of SCKs in these Ag⁺-loaded systems,³⁴ whereas core-loaded SCC10-SCK

NPs are expected to release silver primarily in the form of the SCC molecule. In the event that silver is released as Ag⁺ cations or prematurely dissociated into Ag⁺ cations, there is a likelihood of the silver cations interacting with various anions in the tissue, particularly the Cl⁻ ion, and forming AgCl precipitates. Even though AgCl has been shown to have antimicrobial activity,^{35,36} the low solubility product of AgCl possibly limits the availability of Ag⁺ ions, resulting in an attenuated antimicrobial activity. On the other hand, the coordination of silver to the carbene locks the silver atom in the +1 oxidation state, and upon degradation of the SCC molecule, the silver cation is released. It is likely that there is uptake of SCC by bacterial cells, and subsequent degradation of the SCC molecule within the bacterial cell releases the silver cation, which is responsible for the observed bactericidal effects and superior survival advantage. On the other hand, bacteria are known to utilize two defense mechanisms against heavy metal toxicity: increased expression of heavy metal efflux pumps and up-regulation of antioxidant enzymes.³⁷ While an investigation of the molecular effects of exposure of *P. aeruginosa* strain PA M57-15 to silver is outside the scope of this paper, Yang *et al.* have established a precedent for the biological responses in *P. aeruginosa* strain PAO1 following exposure to heavy metals released from quantum dots (QDs).³⁷ Apart from demonstrating an up-regulation of *czcABC* metal efflux transporters, superoxide dismutase gene *sodM*, and antibiotic resistance (ABR) genes following QD exposure, all of which are findings that can be expected to translate to our SCK NPs, as well, they have shown the formation of biogenic NPs by *P. aeruginosa* following exposure to Cd and Se salts.³⁷ Furthermore, the extracellular synthesis of Se, CdS, and Ag NPs has been demonstrated in a variety of bacteria including *P. aeruginosa* following exposure to the salts of these metals.³⁸⁻⁴¹ These observations demonstrate the possibility of a detoxification mechanism, which results in the removal of released (dissolved) metals within close proximity to the bacteria by chelation by common ligands (chloride, phosphate, sulfides, organic matter, etc.), thus reducing their bioavailability, toxicity, and, in this instance, efficacy.

Additionally, the attachment to and uptake of NPs by bacterial cells may also occur, and subsequently, a controlled delivery of the SCC would occur within the bacterial cell. Several studies document the internalization and accumulation of metal and metal oxide nanoparticles (Ag NPs, ZnO NPs, TiO₂ NPs) in bacterial cells. For instance, Fabrega *et al.* have demonstrated the uptake of silver nanoparticles (Ag NPs) by *Pseudomonas putida* in a biofilm environment,⁴² whereas Morones *et al.* have demonstrated the uptake of Ag NPs by several Gram-negative bacteria such as *Escherichia coli*, *Pseudomonas aeruginosa*, *Vibrio cholera*, and *Salmonella typhus* in planktonic mode.⁴³ Similarly, Kumar *et al.* have demonstrated the internalization of zinc oxide (ZnO) and titanium dioxide (TiO₂) nanoparticles in *E. coli* as well as

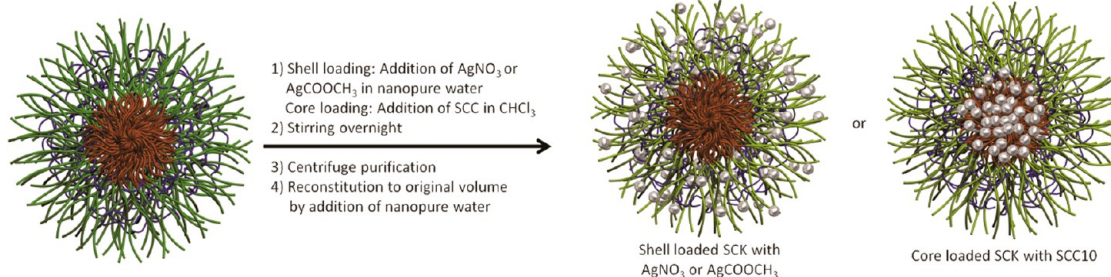


Figure 9. Schematic representation of physical encapsulation of AgNO_3 or AgCOOCH_3 partitioned into the shell of the SCK and silver carbene complex 10 (SCC10) incorporated into the core of the SCK.

TABLE 2. Description of the Clinical Illness Score^a

| clinical parameter | description |
|--------------------|---|
| activity | |
| 0 | normal |
| 1 | slow, but walking |
| 2 | still, moves with gentle nudge with finger |
| 3 | does not move with gentle nudge with finger |
| fur | |
| 0 | smooth |
| 1 | ruffled |
| posture | |
| 0 | normal |
| 1 | hunched |
| 2 | prostrate |

^a The mice were scored for activity, fur, and posture, and the scores for each mouse were pooled. The maximum possible score is 6, which indicates a moribund mouse.

Salmonella typhimurium using flow cytometry and transmission electron microscopy.^{44,45} Even though the precise mechanism for the internalization of nanoparticles in bacteria is unknown, nonspecific diffusion, nonspecific membrane damage, and specific uptake (*si*CBA gene transportation system, through porins) are believed to be possible routes for internalization.⁴⁴ These examples establish the precedent for uptake of nanoparticles by bacterial cells, and even though such data are unavailable for these polymeric SCK NPs, there is likelihood that SCC-bearing SCKs are internalized by bacteria. The occurrence of this phenomenon along with other interactions between the nanoparticles and the bacteria, which define the cellular responses to the NPs and dictate the antimicrobial efficacy, will ultimately depend upon the bacterial “vision” of the NPs. In general, the physicochemical properties of NPs such as composition, shape, size, crystallinity, and structure influence their biomedical application and performance; however, at the same time, they also influence the protein corona at the surface of the NPs.⁴⁶ Ashkarran *et al.* have investigated the bacterial effect on the antimicrobial capability of silver NPs with various geometries on three different types of bacteria and demonstrated that the type of bacteria can have a significant role in the definition of the antimicrobial efficacy of the NPs.⁴⁶ Furthermore, they have demonstrated that the geometry and other physicochemical

properties of the NPs have a considerable impact on the composition and thickness of the protein corona on the NP surface.⁴⁶ The formation of a protein corona at the NP surface is dynamic competitive process^{46,47} that happens instantaneously following the introduction of the nanomaterial into a biological milieu^{48–50} and imparts a new “biological identity” to the NPs.^{51–53} As pointed out by Ashkarran *et al.*, there is a vast difference between what the biological entities actually “see” when interacting with the NPs *versus* the actual pristine surface of the NPs, and significant interplay exists between NP properties, type of bacteria, the biological milieu and the observed antimicrobial efficacy.⁴⁶ Therefore, in the future, the SCK NP formulations will indeed have to be tuned as we develop NP-based therapeutics for the treatment of a variety of different bacteria and transition from *in vitro* to *in vivo* studies.

In the case of the experiments performed with the core-loaded SCK NPs and the dual-loaded SCK NPs, treatment with core-loaded SCK NPs translated to a higher survival advantage than dual-loaded SCK NPs in mice infected with *P. aeruginosa*, despite lower silver loading. For these studies, the differences in the loading and release rate of shell-*versus* core-loaded silver, as well as their individual contribution to the overall therapeutic efficacy, could not be investigated directly using the currently developed formulations due to the inability to distinguish silver release from the core *versus* the shell in the dual-loaded SCK NPs. Therefore, in order to answer this question, which is of considerable importance, we are developing a method wherein, radiolabeled ^{111}Ag will be used to prepare SCC10, which will be subsequently loaded within the core of the nanoparticles, whereas non-radiolabeled Ag^+ cations will be complexed to the shell of the nanoparticles. Since the signal from radiolabeled ^{111}Ag can be differentiated from non-radiolabeled silver, we expect to successfully evaluate the rates of shell—and core—release of silver from the dual-loaded SCK NPs and publish this finding in a future paper. However, the survival data suggest that the dual-loaded SCK NPs have a higher quantity of shell-loaded silver compared with the core-loaded SCC10, thereby resulting in a decreased survival advantage compared with SCC10-only core-loaded SCK NPs. Finally, survival studies were performed with a free-drug formulation of a silver

carbene complex SCC1, a compound we have extensively characterized both *in vitro* and *in vivo*.^{23,25,54,55} These studies demonstrate that a total of 50 mg of SCC1 (14.4 mg of Ag⁺) delivered as five doses of 10 mg of SCC1 (2.88 mg of Ag⁺) each at 12 h intervals were necessary to achieve a 60% survival advantage compared with sham-treated animals. In contrast, a total of 0.88 mg of Ag⁺ delivered as two separate doses (0.44 mg of Ag⁺ each) at 24 h intervals through the core-loaded SCK NP formulation was sufficient to achieve a similar clinical outcome. Thus, a 16-fold higher quantity of the drug was required when administered as a free-drug *via* nebulization to achieve a comparable survival advantage. The superior efficacy of the core-loaded SCK NP formulation can thus be attributed to the sustained delivery of the encapsulated silver carbene complex, which in turn improves the pharmacokinetics of the therapeutic agent *in vivo*.

CONCLUSIONS

We have developed three unique formulations of shell cross-linked nanoparticles (SCK NPs) loaded with

a silver-bearing moiety in either the shell, the core, or both the shell and the core and investigated their efficacy for the treatment of *P. aeruginosa* in a mouse pneumonia model. Our results illustrated that core-loaded and dual-loaded SCK NPs are effective against the CF-relevant bacteria *P. aeruginosa* due to the ability of these nanoparticle formulations to provide a sustained release of the encapsulated silver carbene complex. The ineffectiveness of SCK NPs having only shell loading with AgNO₃ or AgCOOCH₃ is under further investigation and is hypothesized to be due to a relative instability of the weakly complexed Ag⁺ to precipitation with Cl⁻ or other ions and/or reduction to Ag⁰. The use of antimicrobials at high doses raises drug toxicity concerns; however, our data unequivocally demonstrated that such concerns can be alleviated by employing a nanoparticle delivery system allowing depot drug delivery without compromising treatment efficacy. The amphiphilic core–shell morphology of the SCKs is particularly attractive to build up nanoparticle antimicrobial delivery systems of greater complexity and specificity.

MATERIALS AND METHODS

All chemicals were purchased from Sigma-Aldrich Chemical Co. (St. Louis, MO) and used without further purification unless otherwise indicated. Nanopure water (18 MΩ·cm) was acquired by means of a Milli-Q water filtration system (Millipore Corp., Bedford, MA). SCC10 was obtained from Nebusil, Inc. (Akron, OH) and synthesized according to the procedure described by Hindi *et al.*^{27,28} SCK (20% cross-linked, 0.274 mg/mL prepared from PAA₁₂₀-*b*-PS₄₀) was synthesized as previously reported.⁵⁶ The silver-loaded SCK NPs were constructed from aqueous self-assembly of PAA₁₂₀-*b*-PS₄₀ amphiphilic block copolymers into micelles, followed by covalent cross-linking throughout the shell region to afford discrete, robust shell cross-linked nanostructures,⁵⁶ and finally their loading with silver-based antimicrobial agents. The hydrophobic polystyrene core domain is capable of sequestering hydrophobic molecules, and the hydrophilic acrylic acid shell allows for multivalent functionalization, such as cross-linking, complexation with small cationic ions/molecules, or conjugation with chromophores or radiolabels for visualization *in vitro* or tracking *in vivo*. Two procedures were then followed for either shell complexation of silver cation from AgNO₃ or AgCOOCH₃ or core loading of SCC into the SCK NPs (Figure 9). Silver cations were incorporated into the hydrophilic PAA shell region (AgNO₃-SCK, AgCOOCH₃-SCK) by addition of AgNO₃ or AgCOOCH₃ in water into the aqueous SCK NP solution, followed by stirring overnight to afford a homogeneous mixture. SCC10 (silver carbene complex 10, 1-hexyl-3-methyl-4,5-dichloroimidazole-2-ylidene silver(I) acetate, which undergoes decomposition in the presence of saline solution to release active Ag⁺) was encapsulated into the hydrophobic polystyrene core domain and/or the core–shell interface (SCC10-SCK) through addition of SCC10 in chloroform into the aqueous SCK NP solution, followed by stirring and evaporation of the organic solvent at room temperature overnight. In all three cases, free silver was removed using an Amicon ultracentrifugal filter device (100 kDa MWCO, Millipore Corp., Bedford, MA). Sodium chloride was added to the filtrates of AgNO₃-SCK and AgCOOCH₃-SCK until no precipitation was observed to confirm the removal of free silver cations. For SCC10-SCK, UV–visible spectroscopy was used to confirm removal of free SCCs. The resulting silver-loaded SCK NPs were characterized, and their antimicrobial activities were evaluated *in vivo*.

Instrumentation. Ultraviolet–visible spectroscopy (UV–vis) absorption measurements were made using a UV-2550 system (Shimadzu Corp., Japan) with PMMA cuvettes. Inductively coupled plasma-mass spectrometry (ICP-MS) was performed on a Perkin-Elmer SCIEX ICP mass spectrometer ELAN DRC II, equipped with high-speed quadrupole, dynamic reaction cell (DRC), and axial field technology (AFT) to completely eliminate polyatomic interferences, using 1% HNO₃ as the matrix and indium as the internal standard. Dynamic light scattering (DLS) measurements were conducted using Delsa Nano C from Beckman Coulter, Inc. (Fullerton, CA) equipped with a laser diode operating at 658 nm. Size measurements were made in Nanopure water. Scattered light was detected at 15° angle and analyzed using a log correlator over 70 accumulations for 0.5 mL of sample in a glass size cell (0.9 mL capacity). The photomultiplier aperture and the attenuator were automatically adjusted to obtain a photon counting rate of ~10 kcps. The calculation of the particle size distribution and distribution averages was performed using CONTIN particle size distribution analysis routines using Delsa Nano 2.31 software. The peak average of histograms from intensity, volume, and number distributions out of 100 accumulations were reported as the average diameter of the particles, with the standard deviations being calculated as the breadth of the distributions.

Transmission electron microscopy (TEM) bright-field imaging was conducted on a FEI Tecnai G2 F20 FE-TEM, operating at a voltage of 200 kV. The samples were prepared as follows: 4 μL of the dilute solution (with a polymer concentration of ~0.2–0.5 mg/mL) was deposited onto a carbon-coated copper grid, which was pretreated with plasma to increase the surface hydrophilicity. After 5 min, the excess of the solution was quickly wicked away by a piece of filter paper. The samples were then negatively stained with 4 μL of 1 wt % uranyl acetate aqueous solution. After 1 min, the excess uranyl acetate solution was quickly wicked away by a piece of filter paper and the samples were left to dry under ambient conditions overnight. High-resolution scanning transmission electron (STEM) microscopy was conducted on a FEI Tecnai G2 F20 FE-TEM coupled with energy-dispersive X-ray (EDX), operating at a voltage of 200 kV. The samples were prepared as follows: 4 μL of the dilute solution (with a polymer concentration of ~0.2–0.5 mg/mL) was deposited onto a carbon-coated copper grid, which was

pretreated with plasma to increase the surface hydrophilicity. After 5 min, the excess of the solution was quickly wicked away by a piece of filter paper and the samples were left to dry under ambient conditions overnight.

Experimental Procedure. Preparation of Silver Nitrate-Loaded SCK ($\text{AgNO}_3\text{-SCK}$). A solution of AgNO_3 (5.4 mg/mL in Nanopure water, 1.18 mL) was added to the SCK solution (15 mL, polymer concentration = 0.274 mg/mL), and the solution was shielded from light and allowed to stir overnight at room temperature. The solution was transferred to a centrifugal filter device (100 kDa MWCO) and washed with Nanopure water (>3 cycles) to remove free silver and other small molecules. Sodium chloride was added to the filtrate until no precipitation was observed to confirm the removal of free silver ion. The resulting $\text{AgNO}_3\text{-SCK}$ was then reconstituted to a final volume of 15.31 mL, and silver loading concentration was measured by ICP-MS to be 78 ppm.

Preparation of Silver Acetate-Loaded SCK ($\text{AgCOOCH}_3\text{-SCK}$). A solution of AgCOOCH_3 (3.5 mg/mL in Nanopure water, 1.82 mL) was added to the SCK solution (15 mL, polymer concentration = 0.274 mg/mL), and the solution was shielded from light and allowed to stir overnight at room temperature. The solution was transferred to a centrifugal filter device (100 kDa MWCO) and washed with Nanopure water (>3 cycles) to remove free silver and other small molecules. Sodium chloride was added to the filtrate until no precipitation was observed to confirm the removal of free silver ion. The resulting $\text{AgCOOCH}_3\text{-SCK}$ was then reconstituted to a final volume of 15.45 mL, and silver loading concentration was measured by ICP-MS to be 123 ppm.

Preparation of SCC10-Loaded SCK (SCC10-SCK). A solution of SCC10 (6.3 mg/mL in chloroform, 651 μL) was added to the SCK solution (15 mL, polymer concentration = 0.274 mg/mL), and the solution was shielded from light and allowed to stir overnight at room temperature. The solution was transferred to a centrifugal filter device (100 kDa MWCO) and washed with Nanopure water (>3 cycles) to remove free silver and other small molecules. The removal of free silver carbene moieties was confirmed by UV-vis spectroscopy. The resulting SCC10-SCK was then reconstituted to a final volume of 15.63 mL, and silver loading concentration was measured by ICP-MS to be 38 ppm.

Mice. Male C57BL/6J mice (Jackson Laboratories, Bar Harbor, ME) at 6–8 weeks of age were used for these studies. Animals were housed in a barrier facility under pathogen-free conditions until they were inoculated with bacteria. Studies were approved by the University of Texas Southwestern Medical Center and the Washington University School of Medicine IACUC committees.

Drugs and Delivery. SCC10-SCK, $\text{AgNO}_3\text{-SCK}$, $\text{AgCOOCH}_3\text{-SCK}$, SCC10- $\text{AgNO}_3\text{-SCK}$, and empty SCK nanoparticle formulations were always suspended in sterile Nanopure water free of Cl^- ions to avoid the precipitation of AgCl . The nanoparticle formulations were delivered via an Aeroneb Lab apparatus (Aerogen Inc., Galway, Ireland) connected to a multi-dosing animal chamber. The Aerogen nebulizer uses micropump technology to produce fine particles (1–5 μm) in a low velocity aerosol.⁵⁷ The multi-dosing chamber is a square Plexiglas box with inner dimensions of 8 \times 8 \times 4.5 in. height. The nebulizer is mounted in the center of the lid.

Infection Model and Treatment Protocol. A clinical isolate of *P. aeruginosa* designated PA M57-15 was provided by Dr. Thomas Ferkol (Washington University, St. Louis, MO). This isolate is a mucoid strain obtained from a patient with cystic fibrosis and has been extensively studied in animal models.⁵⁸ The bacteria were streaked from glycerol-frozen stocks onto tryptic soy agar (TSA) plates and incubated overnight at 37 °C. Cells from the fresh plate were suspended in Luria (LB) broth (10 mL) to an OD_{650} of 0.2 and grown at 37 °C in a shaking incubator at 200 rpm to an OD_{650} of 0.4, which corresponds to $3.15 \times 10^8 \text{ CFU/mL}$ as determined by serial dilution and plating onto TSA plates.

The first infection model experiment was performed to evaluate and compare the efficacy of the core-only silver-loaded SCK NPs (SCC10-SCK) and the shell-only silver-loaded SCK NPs ($\text{AgNO}_3\text{-SCK}$ and $\text{AgCOOCH}_3\text{-SCK}$). Following anesthesia, mice were

delivered 75 μL of PA M57-15 in LB broth intranasally ($\sim 1.2 \times 10^6 \text{ CFU}$ per mouse). Subsequently, the mice were weighed and randomly assigned to one of the treatment groups. The treatment groups comprised sham treatment (90:10 v/v water/phosphate buffer), blank SCK NPs, SCC10-SCK NPs, $\text{AgNO}_3\text{-SCK}$ NPs, and $\text{AgCOOCH}_3\text{-SCK}$ NPs with 6 mice per group. One hour after inoculation with *P. aeruginosa*, the animals were exposed to a single dose of their respective treatments (15 mL administered over 30 min). To allow nose-only delivery of drug, animals were placed in CH-247 tubes (CH Technologies, Westwood, NJ). Five animals at a time, each housed in individual tubes, were placed into a multi-dosing chamber to administer treatment. Mice were weighed and assigned daily a clinical illness score—an indicator of their health status (Table 2)—as well as observed for survival a total of 72 h after inoculation. The experiment was performed twice, and the data from both experiments have been pooled.

To determine the *in vivo* efficacy of core-loaded silver nanoparticles (SCC10-SCK) versus dual-loaded silver nanoparticles (core and shell, SCC10- $\text{AgNO}_3\text{-SCK}$), the previous mouse model protocol was slightly modified as described below. One hour after inoculation with *P. aeruginosa*, the animals were exposed to a dose of their respective treatments (5 mL administered over 15 min). The treatment groups comprised sham treatment (90:10 v/v water/phosphate buffer), SCC10-SCK nanoparticles, and SCC10- $\text{AgNO}_3\text{-SCK}$ nanoparticles with 5 mice per treatment group. The animals received a second nebulized dose of their respective treatment 24 h after the first. Mice were weighed and scored daily for survival a total of 72 h after inoculation.

In Vivo SCK Delivery, Bronchoalveolar Lavage (BAL), and Quantification of Inflammatory Cells. Mice were anesthetized prior to cannulation of the trachea with a 22-gauge angiocatheter. For intratracheal delivery, sterile phosphate buffered saline (pH 7.4, PBS, Cellgro, Corning Life Science, Corning, NY) alone or SCK (10.8 mg/50 mL) in PBS followed by 50 μL of air as dead space was administered through the catheter as a single bolus. Lungs were subjected to BAL with 1 mL of PBS. BAL fluid was centrifuged, and the cell pellet was resuspended in 1 mL of PBS for total cell count and Cytospin preparation. The immune cell differential was determined using standard light microscopy criteria as described previously.⁵⁹

Statistics. Analyses were performed using Prism 5 (GraphPad Software, Inc., San Diego, CA). The *in vivo* survival curves in the infection model were compared using a log-rank test. To compare the efficacy of shell-loaded SCK nanoparticles with the efficacy of core-loaded SCK nanoparticles, a contingency analysis of the two groups (χ^2) was performed. Changes in animal weights and clinical scores were compared by ANOVA. Comparison of cell counts obtained from bronchoalveolar lavage samples between mice treated with PBS and SCK nanoparticles was performed using a two-tailed *t* test.

Conflict of Interest: The authors declare no competing financial interest.

Acknowledgment: We gratefully acknowledge financial support from the National Heart Lung and Blood Institute of the National Institutes of Health as a Program of Excellence in Nanotechnology (HHSN268201000046C) and the National Science Foundation under Grant No. DMR-1105304. The Welch Foundation is gratefully acknowledged for support through the W.T. Doherty–Welch Chair in Chemistry, Grant No. A-0001.

REFERENCES AND NOTES

1. Lyczak, J. B.; Cannon, C. L.; Pier, G. B. Lung Infections Associated with Cystic Fibrosis. *Clin. Microbiol. Rev.* **2002**, 15, 194–222.
2. Driscoll, J. A.; Brody, S. L.; Kollef, M. H. The Epidemiology, Pathogenesis and Treatment of *Pseudomonas aeruginosa* Infections. *Drugs* **2007**, 67, 351–368.
3. Singh, P. K.; Schaefer, A. L.; Parsek, M. R.; Moninger, T. O.; Welsh, M. J.; Greenberg, E. P. Quorum-Sensing Signals Indicate That Cystic Fibrosis Lungs Are Infected with Bacterial Biofilms. *Nature* **2000**, 407, 762–764.
4. Drenkard, E. Antimicrobial Resistance of *Pseudomonas aeruginosa* Biofilms. *Microbes Infect.* **2003**, 5, 1213–1219.

5. Miali, L. S.; McGinley, N. T.; Brownlee, K. G.; Conway, S. P. Methicillin-Resistant *Staphylococcus aureus* (MRSA) Infection in Cystic Fibrosis. *Arch. Dis. Child.* **2001**, *84*, 160–162.
6. Elizur, A.; Orscheln, R. C.; Ferkol, T. W.; Atkinson, J. J.; Dunne, W. M., Jr.; Buller, R. S.; Armstrong, J. R.; Mardis, E. R.; Storch, G. A.; Cannon, C. L. Panton-Valentine Leukocidin-Positive Methicillin-Resistant *Staphylococcus aureus* Lung Infection in Patients with Cystic Fibrosis. *Chest* **2007**, *131*, 1718–1725.
7. Mahenthiralingam, E.; Baldwin, A.; Vandamme, P. *Burkholderia cepacia* Complex Infection in Patients with Cystic Fibrosis. *J. Med. Microbiol.* **2002**, *51*, 533–538.
8. Marier, J. F.; Brazier, J. L.; Lavigne, J.; Ducharme, M. P. Liposomal Tobramycin against Pulmonary Infections of *Pseudomonas aeruginosa*: A Pharmacokinetic and Efficacy Study Following Single and Multiple Intratracheal Administrations in Rats. *J. Antimicrob. Chemother.* **2003**, *52*, 247–252.
9. Greenberg, D. E.; Marshall-Batty, K. R.; Brinster, L. R.; Zaremba, K. A.; Shaw, P. A.; Mellbye, B. L.; Iversen, P. L.; Holland, S. M.; Geller, B. L. Antisense Phosphorodiamidate Morpholino Oligomers Targeted to an Essential Gene Inhibit *Burkholderia cepacia* Complex. *J. Infect. Dis.* **2010**, *201*, 1822–1830.
10. Wright, J. B.; Lam, K.; Hansen, D.; Burrell, R. E. Efficacy of Topical Silver against Fungal Burn Wound Pathogens. *Am. J. Infect. Control* **1999**, *27*, 344–350.
11. Silver, S.; Phung le, T.; Silver, G. Silver as Biocides in Burn and Wound Dressings and Bacterial Resistance to Silver Compounds. *J. Ind. Microbiol. Biotechnol.* **2006**, *33*, 627–634.
12. Moyer, C. A. Some Effects of 0.5 per cent Silver Nitrate and High Humidity upon the Illness Associated with Large Burns. *J. Natl. Med. Assoc.* **1965**, *57*, 95–100.
13. Melaiye, A.; Youngs, W. J. Silver and Its Application as an Antimicrobial Agent. *Expert Opin. Ther. Pat.* **2005**, *15*, 125–130.
14. Kollef, M. H.; Afessa, B.; Anzueta, A.; Veremakis, C.; Kerr, K. M.; Margolis, B. D.; Craven, D. E.; Roberts, P. R.; Arroliga, A. C.; Hubmayr, R. D.; et al. Silver-Coated Endotracheal Tubes and Incidence of Ventilator-Associated Pneumonia: The Nascent Randomized Trial. *J. Am. Med. Assoc.* **2008**, *300*, 805–813.
15. Gupta, A.; Matsui, K.; Lo, J. F.; Silver, S. Molecular Basis for Resistance to Silver Cations in *Salmonella*. *Nat. Med.* **1999**, *5*, 183–188.
16. Li, X. Z.; Nikaido, H.; Williams, K. E. Silver-Resistant Mutants of *Escherichia coli* Display Active Efflux of Ag⁺ and Are Deficient in Porins. *J. Bacteriol.* **1997**, *179*, 6127–6132.
17. Modak, S. M.; Stanford, J. W.; Bradshaw, W.; Fox, C. L., Jr. Silver Sulfadiazine (AgSD) Resistant *Pseudomonas* Infection in Experimental Burn Wounds. *Panminerva Med.* **1983**, *25*, 181–188.
18. Silver, S. Bacterial Silver Resistance: Molecular Biology and Uses and Misuses of Silver Compounds. *FEMS Microbiol. Rev.* **2003**, *27*, 341–353.
19. Pirnay, J. P.; De Vos, D.; Cochez, C.; Bilocq, F.; Pirson, J.; Struelens, M.; Duinslaeger, L.; Cornelis, P.; Zizi, M.; Vanderkelen, A. Molecular Epidemiology of *Pseudomonas aeruginosa* Colonization in a Burn Unit: Persistence of a Multidrug-Resistant Clone and a Silver Sulfadiazine-Resistant Clone. *J. Clin. Microbiol.* **2003**, *41*, 1192–1202.
20. Sambhy, V.; MacBride, M. M.; Peterson, B. R.; Sen, A. Silver Bromide Nanoparticle/Polymer Composites: Dual Action Tunable Antimicrobial Materials. *J. Am. Chem. Soc.* **2006**, *128*, 9798–9808.
21. Aymonier, C.; Schlotterbeck, U.; Antonietti, L.; Zacharias, P.; Thömann, R.; Tiller, J. C.; Mecking, S. Hybrids of Silver Nanoparticles with Amphiphilic Hyperbranched Macromolecules Exhibiting Antimicrobial Properties. *Chem. Commun.* **2002**, 3018–3019.
22. Mahmoudi, M.; Serpooshan, V. Silver-Coated Engineered Magnetic Nanoparticles Are Promising for the Success in the Fight against Antibacterial Resistance Threat. *ACS Nano* **2012**, *6*, 2656–2664.
23. Kascatan-Nebioglu, A.; Melaiye, A.; Hindi, K.; Durmus, S.; Panzner, M. J.; Hogue, L. A.; Mallett, R. J.; Hovis, C. E.; Coughenour, M.; Crosby, S. D.; et al. Synthesis from Caffeine of a Mixed N-Heterocyclic Carbene-Silver Acetate Complex Active against Resistant Respiratory Pathogens. *J. Med. Chem.* **2006**, *49*, 6811–6818.
24. Kascatan-Nebioglu, A.; Panzner, M. J.; Tessier, C. A.; Cannon, C. L.; Youngs, W. J. N-Heterocyclic Carbene-Silver Complexes: A New Class of Antibiotics. *Coord. Chem. Rev.* **2007**, *251*, 884–895.
25. Panzner, M. J.; Deeraksa, A.; Smith, A.; Wright, B. D.; Hindi, K. M.; Kascatan-Nebioglu, A.; Torres, A. G.; Judy, B. M.; Hovis, C. E.; Hilliard, J. K.; et al. Synthesis and *In Vitro* Efficacy Studies of Silver Carbene Complexes on Biosafety Level 3 Bacteria. *Eur. J. Inorg. Chem.* **2009**, *2009*, 1739–1745.
26. Leid, J. G.; Ditto, A. J.; Knapp, A.; Shah, P. N.; Wright, B. D.; Blust, R.; Christensen, L.; Clemons, C. B.; Wilber, J. P.; Young, G. W.; et al. *In Vitro* Antimicrobial Studies of Silver Carbene Complexes: Activity of Free and Nanoparticle Carbene Formulations against Clinical Isolates of Pathogenic Bacteria. *J. Antimicrob. Chemother.* **2012**, *67*, 138–148.
27. Hindi, K. M.; Siciliano, T. J.; Durmus, S.; Panzner, M. J.; Medvetz, D. A.; Reddy, D. V.; Hogue, L. A.; Hovis, C. E.; Hilliard, J. K.; Mallett, R. J.; et al. Synthesis, Stability, and Antimicrobial Studies of Electronically Tuned Silver Acetate N-Heterocyclic Carbene. *J. Med. Chem.* **2008**, *51*, 1577–1583.
28. Hindi, K. M.; Panzner, M. J.; Tessier, C. A.; Cannon, C. L.; Youngs, W. J. The Medicinal Applications of Imidazolium Carbene-Metal Complexes. *Chem. Rev.* **2009**, *109*, 3859–3884.
29. Patton, J. S.; Fishburn, C. S.; Weers, J. G. The Lungs as a Portal of Entry for Systemic Drug Delivery. *Proc. Am. Thorac. Soc.* **2004**, *1*, 338–344.
30. Meers, P.; Neville, M.; Malinin, V.; Scotto, A. W.; Sardaryan, G.; Kurumunda, R.; Mackinson, C.; James, G.; Fisher, S.; Perkins, W. R. Biofilm Penetration, Triggered Release and *In Vivo* Activity of Inhaled Liposomal Amikacin in Chronic *Pseudomonas aeruginosa* Lung Infections. *J. Antimicrob. Chemother.* **2008**, *61*, 859–868.
31. Hindi, K. M.; Ditto, A. J.; Panzner, M. J.; Medvetz, D. A.; Han, D. S.; Hovis, C. E.; Hilliard, J. K.; Taylor, J. B.; Yun, Y. H.; Cannon, C. L.; et al. The Antimicrobial Efficacy of Sustained Release Silver-Carbene Complex-Loaded L-Tyrosine Polyphosphate Nanoparticles: Characterization, *In Vitro* and *In Vivo* Studies. *Biomaterials* **2009**, *30*, 3771–3779.
32. Pandey, R.; Khuller, G. K. Antitubercular Inhaled Therapy: Opportunities, Progress and Challenges. *J. Antimicrob. Chemother.* **2005**, *55*, 430–435.
33. Thurmond, K. B., II; Kowalewski, T.; Wooley, K. L. Water-Soluble Knedel-like Structures: The Preparation of Shell Crosslinked Small Particles. *J. Am. Chem. Soc.* **1996**, *118*, 7239–7240.
34. Li, Y.; Hindi, K.; Watts, K. M.; Taylor, J. B.; Zhang, K.; Li, Z.; Hunstad, D. A.; Cannon, C. L.; Youngs, W. J.; Wooley, K. L. Shell Crosslinked Nanoparticles Carrying Silver Antimicrobials as Therapeutics. *Chem. Commun.* **2010**, *46*, 121–123.
35. Adams, A. P.; Santschi, E. M.; Mellencamp, M. A. Antibacterial Properties of a Silver Chloride-Coated Nylon Wound Dressing. *Veterinary Surg.* **1999**, *28*, 219–225.
36. Klemencic, D.; Tomsic, B.; Kovac, F.; Simoncic, B. Antimicrobial Cotton Fibres Prepared by *In Situ* Synthesis of AgCl into a Silica Matrix. *Cellulose* **2012**, *19*, 1715–1729.
37. Yang, Y.; Mathieu, J. M.; Chattopadhyay, S.; Miller, J. T.; Wu, T.; Shibata, T.; Guo, W.; Alvarez, P. J. Defense Mechanisms of *Pseudomonas aeruginosa* PAO1 against Quantum Dots and Their Released Heavy Metals. *ACS Nano* **2012**, *6*, 6091–6098.
38. Bai, H. J.; Zhang, Z. M.; Guo, Y.; Yang, G. E. Biosynthesis of Cadmium Sulfide Nanoparticles by Photosynthetic Bacteria *Rhodopseudomonas palustris*. *Colloids Surf., B* **2009**, *70*, 142–146.
39. Kumar, C. G.; Mamidyal, S. K. Extracellular Synthesis of Silver Nanoparticles Using Culture Supernatant of *Pseudomonas aeruginosa*. *Colloids Surf., B* **2011**, *84*, 462–466.

40. Narayanan, K. B.; Sakthivel, N. Biological Synthesis of Metal Nanoparticles by Microbes. *Adv. Colloid Interface Sci.* **2010**, *156*, 1–13.

41. Oremland, R. S.; Herbel, M. J.; Blum, J. S.; Langley, S.; Beveridge, T. J.; Ajayan, P. M.; Sutto, T.; Ellis, A. V.; Curran, S. Structural and Spectral Features of Selenium Nanospheres Produced by Se-Respiring Bacteria. *Appl. Environ. Microbiol.* **2004**, *70*, 52–60.

42. Fabrega, J.; Renshaw, J. C.; Lead, J. R. Interactions of Silver Nanoparticles with *Pseudomonas putida* Biofilms. *Environ. Sci. Technol.* **2009**, *43*, 9004–9009.

43. Morones, J. R.; Elechiguerra, J. L.; Camacho, A.; Holt, K.; Kouri, J. B.; Ramirez, J. T.; Yacaman, M. J. The Bactericidal Effect of Silver Nanoparticles. *Nanotechnology* **2005**, *16*, 2346–2353.

44. Kumar, A.; Pandey, A. K.; Singh, S. S.; Shanker, R.; Dhawan, A. Cellular Uptake and Mutagenic Potential of Metal Oxide Nanoparticles in Bacterial Cells. *Chemosphere* **2011**, *83*, 1124–1132.

45. Kumar, A.; Pandey, A. K.; Singh, S. S.; Shanker, R.; Dhawan, A. A Flow Cytometric Method To Assess Nanoparticle Uptake in Bacteria. *Cytometry, Part A* **2011**, *79*, 707–712.

46. Ashkarran, A. A.; Ghavami, M.; Aghaverdi, H.; Stroeve, P.; Mahmoudi, M. Bacterial Effects and Protein Corona Evaluations: Crucial Ignored Factors in the Prediction of Bioefficacy of Various Forms of Silver Nanoparticles. *Chem. Res. Toxicol.* **2012**, *25*, 1231–1242.

47. Mahmoudi, M.; Sant, S.; Wang, B.; Laurent, S.; Sen, T. Superparamagnetic Iron Oxide Nanoparticles (Spions): Development, Surface Modification and Applications in Chemotherapy. *Adv. Drug Delivery Rev.* **2011**, *63*, 24–46.

48. Mahmoudi, M.; Lynch, I.; Ejtehadi, M. R.; Monopoli, M. P.; Bombelli, F. B.; Laurent, S. Protein–Nanoparticle Interactions: Opportunities and Challenges. *Chem. Rev.* **2011**, *111*, 5610–5637.

49. Monopoli, M. P.; Walczyk, D.; Campbell, A.; Elia, G.; Lynch, I.; Bombelli, F. B.; Dawson, K. A. Physical–Chemical Aspects of Protein Corona: Relevance to *In Vitro* and *In Vivo* Biological Impacts of Nanoparticles. *J. Am. Chem. Soc.* **2011**, *133*, 2525–2534.

50. Walczyk, D.; Bombelli, F. B.; Monopoli, M. P.; Lynch, I.; Dawson, K. A. What the Cell “Sees” in Bionanoscience. *J. Am. Chem. Soc.* **2010**, *132*, 5761–5768.

51. Cedervall, T.; Lynch, I.; Foy, M.; Berggard, T.; Donnelly, S. C.; Cagney, G.; Linse, S.; Dawson, K. A. Detailed Identification of Plasma Proteins Adsorbed on Copolymer Nanoparticles. *Angew. Chem., Int. Ed.* **2007**, *46*, 5754–5756.

52. Cedervall, T.; Lynch, I.; Lindman, S.; Berggard, T.; Thulin, E.; Nilsson, H.; Dawson, K. A.; Linse, S. Understanding the Nanoparticle–Protein Corona Using Methods To Quantify Exchange Rates and Affinities of Proteins for Nanoparticles. *Proc. Natl. Acad. Sci. U.S.A.* **2007**, *104*, 2050–2055.

53. Kim, J. A.; Aberg, C.; Salvati, A.; Dawson, K. A. Role of Cell Cycle on the Cellular Uptake and Dilution of Nanoparticles in a Cell Population. *Nat. Nanotechnol.* **2012**, *7*, 62–68.

54. Cannon, C. L.; Hogue, L. A.; Vajravelu, R. K.; Capps, G. H.; Ibricevic, A.; Hindi, K. M.; Kascatan-Nebioglu, A.; Walter, M. J.; Brody, S. L.; Youngs, W. J. *In Vitro* and Murine Efficacy and Toxicity Studies of Nebulized SCC1, a Methylated Caffeine–Silver(I) Complex, for Treatment of Pulmonary Infections. *Antimicrob. Agents Chemother.* **2009**, *53*, 3285–3293.

55. Panzner, M. J.; Hindi, K. M.; Wright, B. D.; Taylor, J. B.; Han, D. S.; Youngs, W. J.; Cannon, C. L. A Theobromine Derived Silver N-Heterocyclic Carbene: Synthesis, Characterization, and Antimicrobial Efficacy Studies on Cystic Fibrosis Relevant Pathogens. *Dalton Trans.* **2009**, *7308–7313*.

56. Lin, L. Y.; Lee, N. S.; Zhu, J.; Nystrom, A. M.; Pochan, D. J.; Dorshow, R. B.; Wooley, K. L. Tuning Core vs. Shell Dimensions To Adjust the Performance of Nanoscopic Containers for the Loading and Release of Doxorubicin. *J. Controlled Release* **2011**, *152*, 37–48.

57. Geller, D. E.; Rosenfeld, M.; Waltz, D. A.; Wilmott, R. W. Efficiency of Pulmonary Administration of Tobramycin Solution for Inhalation in Cystic Fibrosis Using an Improved Drug Delivery System. *Chest* **2003**, *123*, 28–36.

58. van Heeckeren, A. M.; Tscheikuna, J.; Walenga, R. W.; Konstan, M. W.; Davis, P. B.; Erokwu, B.; Haxhiu, M. A.; Ferkol, T. W. Effect of *Pseudomonas* Infection on Weight Loss, Lung Mechanics, and Cytokines in Mice. *Am. J. Respir. Crit. Care Med.* **2000**, *161*, 271–279.

59. Gunsten, S.; Mikols, C. L.; Grayson, M. H.; Schwendener, R. A.; Agapov, E.; Tidwell, R. M.; Cannon, C. L.; Brody, S. L.; Walter, M. J. IL-12 P80-Dependent Macrophage Recruitment Primes the Host for Increased Survival Following a Lethal Respiratory Viral Infection. *Immunology* **2009**, *126*, 500–513.